

Fabrication and structural properties of AlN submicron periodic lateral polar structures and waveguides for UV-C applications

D. Alden,^{1,2} W. Guo,¹ R. Kirste,³ F. Kaess,¹ I. Bryan,¹ T. Troha,⁴ A. Bagal,⁵ P. Reddy,¹ Luis H. Hernandez-Balderrama,¹ A. Franke,¹ S. Mita,³ C.-H. Chang,⁵ A. Hoffmann,² M. Zgonik,⁴ R. Collazo,¹ and Z. Sitar¹

¹Department of Materials Science and Engineering, North Carolina State University, Raleigh, North Carolina 27695, USA

²Institut für Festkörperphysik, Technische Universität Berlin, Hardenbergstr. 36, 10623 Berlin, Germany

³Adroit Materials, Inc., 2054 Kildaire Farm Rd., Suite 205, Cary, North Carolina 27518, USA

⁴Faculty of Mathematics and Physics, University of Ljubljana, Jadranska 19, 1000 Ljubljana, Slovenia

⁵Department of Mechanical and Aerospace Engineering, North Carolina State University, Raleigh, North Carolina 27695, USA

(Received 31 March 2016; accepted 18 June 2016; published online 30 June 2016)

Periodically poled AlN thin films with submicron domain widths were fabricated for nonlinear applications in the UV-VIS region. A procedure utilizing metalorganic chemical vapor deposition growth of AlN in combination with laser interference lithography was developed for making a nanoscale lateral polarity structure (LPS) with domain size down to 600 nm. The Al-polar and N-polar domains were identified by wet etching the periodic LPS in a potassium hydroxide solution and subsequent scanning electron microscopy (SEM) characterization. Fully coalesced and well-defined vertical interfaces between the adjacent domains were established by cross-sectional SEM. AlN LPSs were mechanically polished and surface roughness with a root mean square value of ~10 nm over a 90 $\mu\text{m} \times 90 \mu\text{m}$ area was achieved. 3.8 μm wide and 650 nm thick AlN LPS waveguides were fabricated. The achieved domain sizes, surface roughness, and waveguides are suitable for second harmonic generation in the UVC spectrum. Published by AIP Publishing.

[<http://dx.doi.org/10.1063/1.4955033>]

Lasers emitting in the ultraviolet spectrum are desired for a variety of applications, including photochemical labeling, biosensing, nanolithography, medical surgery, micromachining, Bragg gratings, and many others. Currently available UV laser systems are expensive, inefficient, stationary, large, and require frequent maintenance. Although many advances have been made toward the fabrication of electrically injected AlGaN semiconductor based UV-C laser diodes, doping, carrier injection, and defect control are still challenging.^{1–3}

An alternative approach to compact UV-C lasers is to exploit frequency doubling via second harmonic generation (SHG). When conventional birefringence phase matching is not possible, a quasi phase matching (QPM) approach is necessary. For efficient QPM, a structure is needed in which the orientation of the nonlinear susceptibility coefficient is periodically inverted. In polar materials this can be achieved either by electrical poling or by growing periodically oriented lateral polarity structures (LPS). Single pass conversion efficiencies of up to 83% have been reported using QPM in the VIS-IR region by employing periodically poled nonlinear crystals.⁴ Moreover, QPM has numerous advantages over birefringence phase matching from a practical point of view and allows for many applications involving other nonlinear optical processes detailed in Ref. 5. Even though significant advances have been made in nanoscale periodic poling of ferroelectric materials, QPM SHG in the UV range presents several challenges.^{6,7} Prominent materials used for QPM applications, like periodically poled LiNbO₃ and LiTaO₃, lack transparency in the UV-C range and present difficulties in achieving poling periods on the order of a few hundred

nm needed for UV applications. AlN is an excellent candidate for the generation of UV-C laser light via QPM and a variety of other nonlinear optical applications due to its large second order nonlinear susceptibility coefficient along the c-axis of 7.7 pm/V, high thermal conductivity (320 W/mK), and a wide transparency window (205 nm and above). This enables the possibility for high conversion efficiency, high power damage threshold, and wide wavelength tunability.^{8–10} There have been attempts to grow periodically poled AlN by molecular beam epitaxy on the submicron scale utilizing Mg doping and E-beam lithography coupled with regrowth.¹¹ This polarity control scheme led to trenches at the polar domain interfaces due to the high aspect ratios between the polar domains during regrowth. This in turn hindered the application for SHG by QPM due to high scattering losses. The growth of AlN via metalorganic chemical vapor deposition (MOCVD) allows for on-chip, small-scale integrated devices, making it a very attractive technique for the fabrication of LPS for QPM. It has been previously shown that the polarity of III-nitride thin films deposited on sapphire substrates is III-polar when grown on a properly annealed AlN nucleation layer deposited at low temperature (650 °C). When deposited on sapphire without previously depositing a nucleation layer, the polarity is N-polar.^{12–15} Only domain sizes down to 5 μm were demonstrated due to the limitations in the patterning process. Thus, new methods are needed to provide finer long-range periodicities that can be used for QPM in the UV-C.

In this work, the fabrication of AlN lateral polar structures (LPS) with varying thicknesses and periodicities suitable

for QPM in the UV-C range is described. Fully coalesced films, well-defined interfaces at the inversion domain boundary (IDB), and uniform polarity within the alternating domains were demonstrated. The LPS were mechanically polished to reduce the surface roughness and waveguides were etched perpendicular to the AlN LPS.

AlN lateral polarity structures were fabricated via substrate patterning and subsequent simultaneous MOCVD growth of both domains. The process used in this work is shown in Figure 1 and was developed based on previous work.^{16,17} The films grown are deposited via MOCVD in a vertical cold-walled reactor with a background pressure of 8×10^{-7} Torr. First, a 20 nm aluminum nitride nucleation layer is deposited on an LED-quality c-plane sapphire substrate at 650 °C. The substrate is then removed from the reactor and spin-coated with a 100 nm thick anti-reflection coating (ARC) and a 700 nm thick photoresist layer. The sub-micrometer pattern needed for the UV-C nonlinear applications is obtained using laser interference lithography in a Lloyd's mirror configuration, resulting in a highly periodic sub-micrometer pattern across the entire substrate. For this, a He-Cd laser focused onto a pinhole is used as a monochromatic point light source. The sample is placed adjacent to a fixed 90° mirror acting as the second light source with the same incidence angle θ . The periodicity, Λ , of the interference pattern is then defined by the angle of incidence θ with respect to the normal of the sample, the wavelength λ of the light source, and the refractive index n of the medium as follows:

$$\Lambda = \frac{\lambda}{2n \sin \theta}.$$

This patterning process allows for periodicities down to 200 nm in air and even lower when immersed in an appropriate liquid with a higher refractive index. More details on the employed setup can be found elsewhere.¹⁸ The pattern was transferred to the ARC layer by reactive ion etching (RIE) in oxygen plasma for 3 min at an RF power of 54 W, 30 sccm of O₂ flow under a total pressure of 30 mTorr, using a Semigroupt 1000TP system. The pattern was then transferred

to the AlN nucleation layer by RIE in a Minilock II Reactive Ion Etching system. For the latter, the samples were etched for 5 min at an RF power of 100 W in a gas mixture of 25 sccm BCl₃ and 25 sccm Cl₂ under a total chamber pressure of 75 mTorr. The remaining photoresist residue was then removed by isotropic O₂ plasma in a PM-600 system.

The substrate is then placed in the reactor where it is vacuum annealed at 1040 °C for 10 min. Thereafter, the reactor is backfilled with H₂ to a reactor total pressure of 20 Torr and maintained at 1040 °C for an additional 7 min. Next, the temperature is lowered to 950 °C and the sample is exposed to a mixture of 1 slm N₂ and 1 slm NH₃ for 4 min. The substrate temperature is then increased to 1100 °C where the AlN growth is started by flowing 6.7 μmol/min of trimethylaluminium (TMA) and 0.3 slm NH₃ for 10 min using N₂ as the precursor carrier gas and 10 slm of H₂ as a diluent gas in a reactor total pressure of 80 Torr. Finally, the temperature and the TMA flow are increased to 1250 °C and 13.4 μmol/min, respectively. In this process, N-polar domains grow on the bare sapphire regions and Al-polar domains on the AlN nucleation layer.¹³ Both polarities grow simultaneously, forming a seamless inversion domain boundary (IDB).

The surface and domain boundaries of the patterned substrates before and after AlN film deposition, as displayed in step 5 and step 6 in Fig. 1 respectively, were analyzed in an Asylum Research MFP-3D atomic force microscope (AFM). Subsequently, cross-section Secondary Electron Microscopy (SEM) images were taken in a Verios 460L FEI system to determine the total thickness of the samples and to confirm the polarity of the AlN LPS. For the latter, a sample was submerged in a 1 molar concentration of potassium hydroxide (KOH) solution in deionized (DI) water for 1 min at 70 °C.¹⁹

In order to reduce the surface roughness, the AlN LPS was mechanically polished utilizing 1 μm–0.25 μm diamond lapping film. The AlN LPS samples were characterized by AFM before and after mechanical polishing. Finally, rectangular waveguides were etched into the polished AlN LPS using conventional photolithography.

AFM images of the patterned substrate before and after the AlN film deposition are shown in Figures 2(a) and 2(b). In Figure 2(a), alternating stripes of low temperature AlN

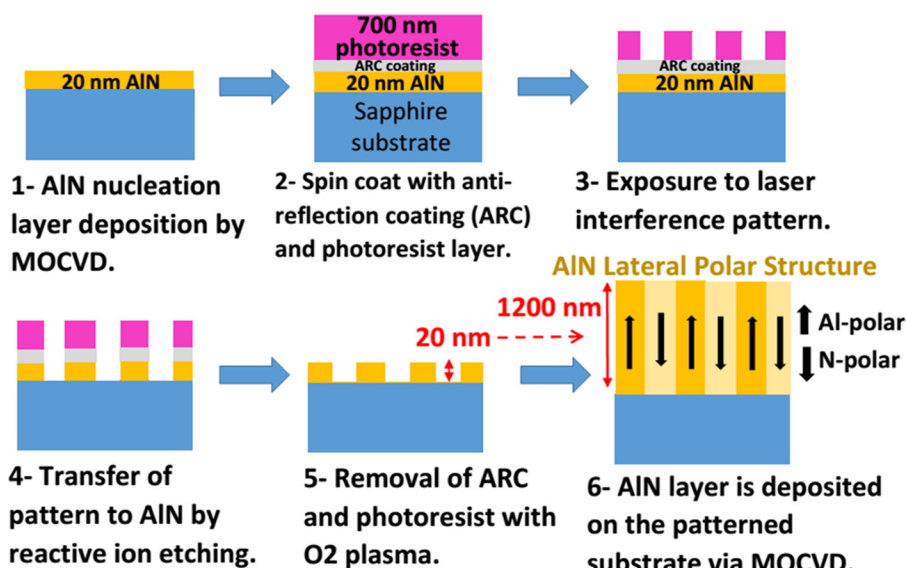


FIG. 1. Nanoscale polarity control process scheme. Step 1: MOCVD deposition of AlN nucleation layer on c-plane sapphire. Step 2: Photoresist and ARC are spin coated onto the substrate. Step 3: Photoresist layer is exposed to the laser interference periodic pattern and developed. Step 4: Pattern is transferred to the AlN nucleation layer by reactive ion etching. Step 5: The residual photoresist and ARC are removed by O₂ plasma. Step 6: The patterned substrate is reinserted in the MOCVD chamber, where the AlN film is deposited leading to the AlN periodic lateral polar structure.

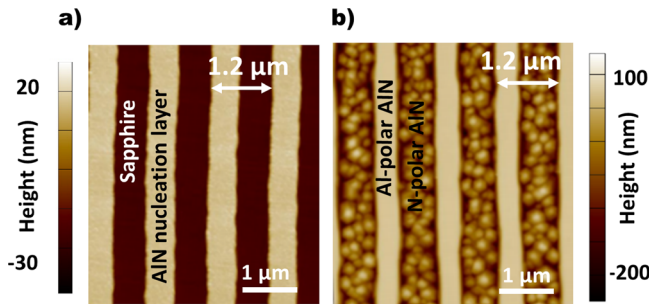


FIG. 2. Height profile AFM images of the patterned substrate before (a) and after the AlN thin film growth (b). The patterned AlN/sapphire substrate with a $1.2\text{ }\mu\text{m}$ periodicity is shown. High color contrast at the interfaces is observed indicating an abrupt change in height. (b) The alternating N-polar and Al-polar domains of a $1\text{ }\mu\text{m}$ thick LPS are displayed. A rough hexagonal columnar surface characteristic of the N-polar domain is observed as well as a smooth (sub-nanometer RMS roughness) Al-polar surface with similar domain sizes as the patterned substrate, pointing at the vertical inversion domain boundaries.

nucleation layer and bare sapphire substrate can be observed. The step height between the stripes is about 20 nm, which is consistent with the thickness of the nucleation layer. Figure 2(b) shows an image of a $1\text{ }\mu\text{m}$ thick AlN film deposited on to this patterned substrate. Two different stripes of similar width to the initial pattern are observed and identified as Al- and N-polar domains. The surface morphology for the Al-polar domains is smooth, while columnar hexagonal structures are observed for the N-polar AlN, which is typical behavior of the respective polarities at these growth conditions.¹³ The inversion domain boundary between the Al- and N-polar domains is well defined which demonstrates the ability to apply sub-micron patterning using interference lithography.

AlN LPS with a periodicity of $1.2\text{ }\mu\text{m}$ are intended for QPM SHG at 275 nm for a 650 nm thick and $5\text{ }\mu\text{m}$ wide rectangular waveguide. The coherence length was calculated using Marcatili's approach;²⁰ the Sellmeier's parameters for AlN were taken from Ref. 21. We have also demonstrated AlN LPS with periodicities ranging from 400 nm up to $6\text{ }\mu\text{m}$ (not shown), which allows for tunability of the SHG wavelength from 200 nm up to 550 nm, thereby enabling QPM over the whole transparency range of AlN.

In order to estimate the layer thickness and assess its uniformity, the samples were cleaved perpendicular to the alternating polar domains and cross-sectional SEM was performed. Figures 3(a)–3(c) show cross sectional SEM

images for the 400 nm, 700 nm, and 1000 nm thick structures, respectively.

Using 47 mJ of light exposure dose, 3 min RIE in oxygen plasma, and 5 min RIE in BCl_3 and Cl_2 under the conditions described previously resulted in domains of similar width (Figures 3(b) and 3(c)). The polar domains are fully coalesced at the IDBs, which are highlighted by the yellow dashed lines. This result is supported by Transmission Electron Microscopy (TEM) and Scanning Transmission Electron Microscopy (STEM) studies discussed elsewhere.²² The smooth plateaus are characteristic of the Al-polar domains while the rougher surface with triangular tips is representative of the N-polar domains. The 20 nm patterned low temperature AlN nucleation layer can also be observed, which, as expected, is present directly below the plateaus of the Al-polar domains. In contrast to other semiconductors where different growth rates between the polar domains may lead to significant height differences and even lateral overgrowth of one polarity over the other, AlN grown under the applied conditions has equal growth rates for both polar directions as can be inferred from the cross-section SEM images. This is key for vertical and well-coalesced interfaces of the periodically poled AlN, which are essential for SHG by QPM.²³

In order to unambiguously identify the Al-polar and N-polar domains as well as to identify any inversion domains within the stripes, as they could be detrimental for QPM, KOH etching and subsequent SEM characterization were performed.¹⁹ Figure 4 shows tilted cross-section SEM images of the sample after the AlN film deposition (a) and the same sample after etching in a 1M KOH solution in deionized water for 1 min at 70°C . For the wet etched sample, the N-polar domains were completely removed while the Al-polar domains remained unetched, thereby confirming the polarity of the respective domains.¹⁹ Some lateral etching is observed at the Al-polar domains; however, no vertical top-down etching is observed.

For QPM, the excitation and second harmonic light travel in the AlN waveguides and scattering losses will depend on surface roughness. This seems a concern mainly for the N-polar AlN domains (Figure 2(b)). No scattering is expected at the inversion domain boundary because of the same refractive index of the N- and Al-polar material.²¹ Surface scattering losses due to random deviations at the waveguide boundaries have been investigated in detail.^{24,25}

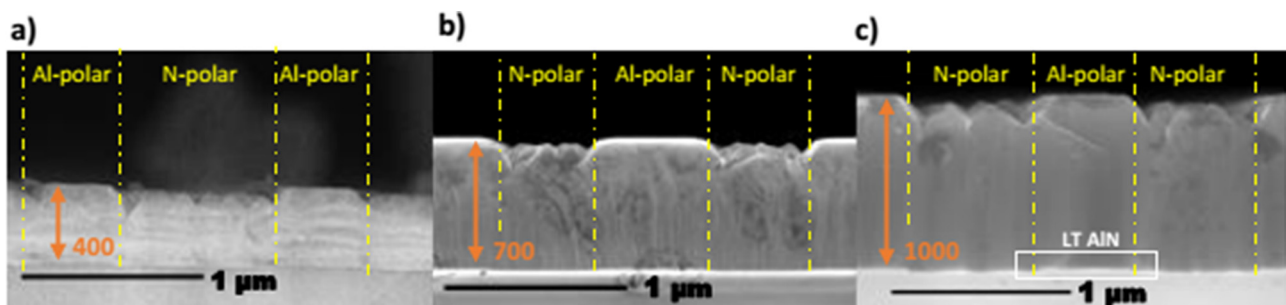


FIG. 3. Cross-sectional SEM images of samples of various thicknesses. The inversion domain boundaries are highlighted with yellow dashed lines. Complete coalescence at the IDBs is observed. Similar growth rates for both polarities are measured, and a linear increase of the film thickness with increasing deposition time is determined as expected for the mass transport limited growth regime.

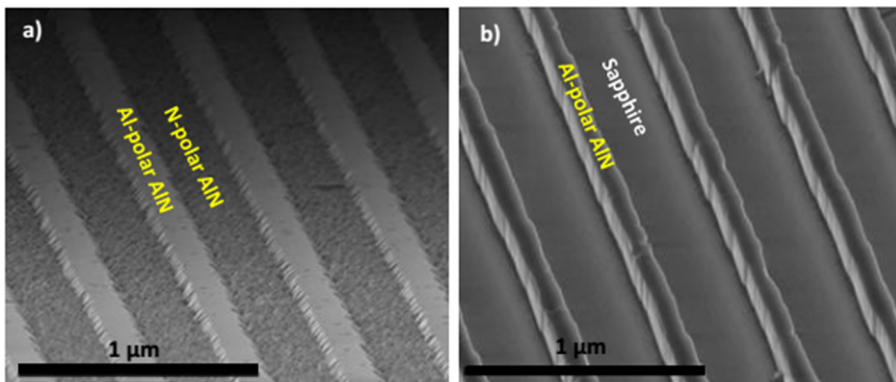


FIG. 4. Tilted view SEM image of the AlN LPS as grown (a) and after being submerged in a 1 molar KOH solution in deionized water for 1 min at 70 °C (b). The N-polar domains were completely etched away while the Al-polar regions remained nearly unchanged, confirming the alternating polarity of the structure. Some sidewall etching is determined at the Al-polar domains from the reduced domains' width; however, no top-down etching is observed as expected for the +C polar direction.

Under the Rayleigh criterion, a surface may be considered as smooth for

$$\sigma_s < \frac{\lambda}{8 \cos \theta},$$

where σ_s is the root mean square (RMS) surface roughness, λ is the wavelength in the material, and θ the angle of incidence. To obtain θ_m (angle of incidence for the m th-order TM mode in the guiding layer), one needs to solve the transcendental equation

$$\tan(ht) = \frac{h(p+q)}{h^2 - pq},$$

for the propagation constant β (Equation (3.16) in Ref. 26, p. 36), where t is the waveguide thickness, and q and p the extinction coefficients in the confining layers with

$$q = \frac{n_2^2}{n_1^2} (\beta^2 - n_1^2 k^2)^{\frac{1}{2}}, \quad p = \frac{n_2^2}{n_1^2} (\beta^2 - n_3^2 k^2)^{\frac{1}{2}} \quad \text{and}$$

$$h = (n_2^2 k^2 - \beta^2)^{\frac{1}{2}},$$

k is the wavenumber in vacuum and n_1, n_2, n_3 are the refractive indices of air, AlN, and sapphire, respectively. Like p and q , h is a constant determined by the boundary conditions and is also given in terms of β . The propagation constant β is then related to θ_m through

$$\beta = kn_2 \sin \theta_m.$$

For a waveguide thickness of 650 nm, refractive indices at 550 nm (pump wavelength) of 2.13 and 1.77 for AlN and sapphire, respectively,^{21,27} the angle of incidence θ_m for the highest order mode ($m=2$) is calculated to be 57.4°. This leads to a maximum allowed surface roughness RMS value of ~60 nm for the Rayleigh criterion to hold true.

The RMS surface roughness over a $90 \times 90 \mu\text{m}^2$ area of the grown samples was determined to be ~30 nm, regardless of thickness. Utilizing the method in Ref. 24, the scattering losses at the surface α_s are calculated to be around 100 cm^{-1} for the 0th order TM mode.

In Figure 5(a), an AFM topograph is displayed after the mechanical polishing; Figures 5(b) and 5(c) show typical line scans taken from AlN LPS films and mechanically polished AlN LPS films, respectively. The mechanically polished

samples showed significantly improved RMS surface roughness values of 10–15 nm. Further reduction of the roughness is challenging as longer polishing times did not lead to further improvement. This may have stem from the polarity-dependent etching due to the pH of the polishing vehicle. Nevertheless, the achieved RMS roughness values were well below the Rayleigh criterion limit and the scattering losses, α_s , for the 0th order TM mode were calculated to be around 10 cm^{-1} at 550 nm and 6 cm^{-1} for the SHG wave at 275 nm.^{21,27} These values confirm that the fabricated AlN LPS are suitable for SHG in the UV-C spectrum.

Finally, rectangular waveguides were fabricated using standard photolithography and RIE in Cl_2 and BCl_3 , as shown in Figure 6. They were 650 nm thick and $3.8 \mu\text{m}$ wide as determined by AFM (not shown) and SEM measurements. The lateral polar structure along the waveguide is clearly observed, highlighted by the difference in the surface roughness between the Al- and N-polar domains. Similar to the AFM image in Figure 5, it is observed that the N-polar surface is significantly rougher than the Al-polar. However, it is clear from the sidewall that the bulk of the film is well-coalesced within both domains as well as at the IDB. In addition, vertical and smooth sidewalls were obtained. The inset shows a low magnification SEM image of a large area with multiple AlN LPS waveguides, highlighting one of the advantages of the fabrication process employed here over other patterning techniques such as electron-beam lithography. It is important to note that due to the nature of the laser interference in the patterning process, the periodicity is maintained over the entire pattern, which is crucial to avoid long range period errors that could be detrimental to the efficiency of QPM-SHG.

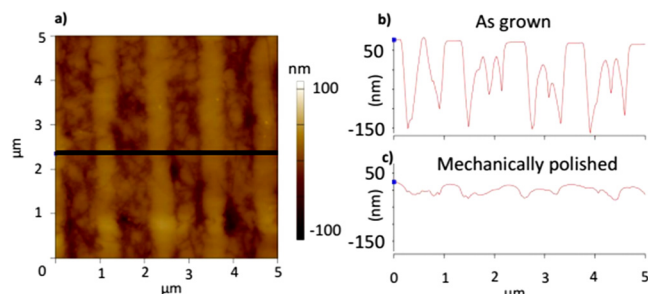


FIG. 5. AFM topograph of an AlN LPS after mechanical polishing (a) and a line scan perpendicular to the stripe direction before (b) and after polishing (c).

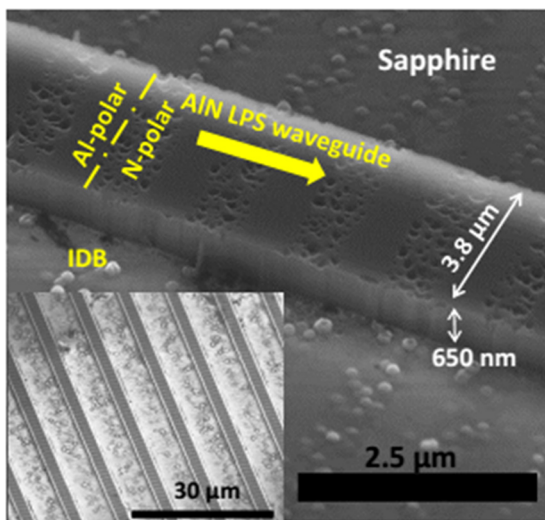


FIG. 6. SEM image of the first AlN LPS waveguides. The alternating polarity along the waveguide is observed, with the characteristic roughness of the N-polar domains. Also the well-coalesced interface between the polar domains can be seen. The inset shows a larger area scan with multiple waveguides.

In summary, large area, highly periodic, submicrometer AlN lateral polar structures were fabricated. Mechanical polishing resulted in an improved surface morphology with RMS roughness of ~ 10 nm, as determined by AFM. Finally, the first LPS-based AlN waveguides were fabricated using standard photolithography and RIE. Having well-defined and coalesced interfaces at the IDBs and low scattering losses at the waveguide surface (calculated $\alpha_s < 10 \text{ cm}^{-1}$), these waveguides are suitable for efficient second harmonic generation in the UV-C spectrum by quasi phase matching.

Partial financial support from NSF (DMR-1312582, DMR-1108071, and DMR-1508191), and ARO (W911NF-04-D-003-0014 and W911NF-15-2-0068) is greatly appreciated. Furthermore, D. Alden would like to acknowledge CONACYT-Mexico for their financial support, and A. Franke would like to acknowledge the National Research Council Research fellowship.

¹Z. Bryan, I. Bryan, B. E. Gaddy, P. Reddy, L. Hussey, M. Bobea, W. Guo, M. Hoffmann, R. Kirste, J. Tweedie, M. Gerhold, D. L. Irving, Z. Sitar, and R. Collazo, "Fermi level control of compensating point defects during metalorganic chemical vapor deposition growth of Si-doped AlGaN," *Appl. Phys. Lett.* **105**, 222101 (2014).

²W. Guo, Z. Bryan, J. Xie, R. Kirste, S. Mita, I. Bryan, L. Hussey, M. Bobea, B. Haidet, M. Gerhold, R. Collazo, and Z. Sitar, "Stimulated emission and optical gain in AlGaN heterostructures grown on bulk AlN substrates," *J. Appl. Phys.* **115**, 103108 (2014).

³M. T. Hardy, D. F. Feezell, S. P. Denbaars, and S. Nakamura, "Group III-nitride lasers: A materials perspective," *Mater. Today* **14**(9), 408–415 (2011).

⁴D. Taverner, P. Britton, P. G. Smith, D. J. Richardson, G. W. Ross, and D. C. Hanna, "Highly efficient second-harmonic and sum-frequency generation of nanosecond pulses in a cascaded erbium-doped fiber: Periodically poled lithium niobate source," *Opt. Lett.* **23**(3), 162–164 (1998).

⁵D. S. Hum and M. M. Fejer, "Quasi-phasematching," *C. R. Phys.* **8**(2), 180–198 (2007).

⁶J. P. Meyn, C. Laue, R. Knappe, R. Wallenstein, and M. M. Fejer, "Fabrication of periodically poled lithium tantalate for UV generation with diode lasers," *Appl. Phys. B: Lasers Opt.* **73**(2), 111–114 (2001).

⁷K. Mizuchi, A. Morikawa, T. Sugita, and K. Yamamoto, "Efficient second-harmonic generation of 340-nm light in a 1.4- μm periodically poled bulk MgO:LiNbO₃," *Jpn. J. Appl. Phys., Part 2* **42**(2A), L90–L91 (2003).

⁸Y. Fujii, S. Yoshida, S. Misawa, S. Maekawa, and T. Sakudo, "Nonlinear optical susceptibilities of AlN film," *Appl. Phys. Lett.* **31**(12), 815–816 (1977).

⁹G. A. Slack, R. Tanzilli, R. Pohl, and J. Vandersande, "The intrinsic thermal conductivity of AlN," *J. Phys. Chem. Solids* **48**(7), 641–647 (1987).

¹⁰M. Strassburg, J. Senawiratne, N. Dietz, U. Haboeck, A. Hoffmann, V. Noveski, R. Dalmau, R. Schlesser, and Z. Sitar, "The growth and optical properties of large, high-quality AlN single crystals," *J. Appl. Phys.* **96**(10), 5870–5876 (2004).

¹¹J. Wright, C. Moe, A. V. Sampath, G. A. Garrett, and M. Wraback, "Fabrication of periodically poled AlN with sub-micron periods," *Phys. Status Solidi C* **8**(7–8), 2331–2333 (2011).

¹²F. Liu, R. Collazo, S. Mita, Z. Sitar, G. Duscher, and S. J. Pennycook, "The mechanism for polarity inversion of GaN via a thin AlN layer: Direct experimental evidence," *Appl. Phys. Lett.* **91**, 203115 (2007).

¹³R. Kirste, S. Mita, L. Hussey, M. P. Hoffmann, W. Guo, I. Bryan, Z. Bryan, J. Tweedie, J. Xie, M. Gerhold, R. Collazo, and Z. Sitar, "Polarity control and growth of lateral polarity structures in AlN," *Appl. Phys. Lett.* **102**, 181913 (2013).

¹⁴M. Stutzmann, O. Ambacher, M. Eickhoff, U. Karrer, A. L. Pimenta, R. Neuberger, J. Schalwig, R. Dimitrov, P. J. Schuck, and R. D. Grober, "Playing with polarity," *Phys. Status Solidi B* **228**(2), 505–512 (2001).

¹⁵J. K. Hite, N. D. Bassim, M. E. Twigg, M. A. Mastro, F. J. Kub, and C. R. Eddy, "GaN vertical and lateral polarity heterostructures on GaN substrates," *J. Cryst. Growth* **332**(1), 43–47 (2011).

¹⁶R. Collazo, S. Mita, A. Aleksov, R. Schlesser, and Z. Sitar, "Growth of Ga- and N-polar gallium nitride layers by metalorganic vapor phase epitaxy on sapphire wafers," *J. Cryst. Growth* **287**(2), 586–590 (2006).

¹⁷R. Collazo, S. Mita, A. Rice, R. F. Dalmau, and Z. Sitar, "Simultaneous growth of a GaN p/n lateral polarity junction by polar selective doping," *Appl. Phys. Lett.* **91**(21), 212103 (2007).

¹⁸A. Bagal and C.-H. Chang, "Fabrication of subwavelength periodic nanostructures using liquid immersion Lloyd's mirror interference lithography," *Opt. Lett.* **38**(14), 2531–2534 (2013).

¹⁹W. Guo, R. Kirste, I. Bryan, Z. Bryan, L. Hussey, P. Reddy, J. Tweedie, R. Collazo, and Z. Sitar, "KOH based selective wet chemical etching of AlN, Al_xGa_{1-x}N, and GaN crystals: A way towards substrate removal in deep ultraviolet-light emitting diode," *Appl. Phys. Lett.* **106**, 082110 (2015).

²⁰E. A. J. Marcatili, "Dielectric rectangular waveguide and directional coupler for integrated optics," *Bell Syst. Technol. J.* **48**(7), 2071–2102 (1969).

²¹M. Rigler, J. Buh, M. Hoffmann, R. Kirste, M. Bobea, S. Mita, M. Gerhold, R. Collazo, Z. Sitar, and M. Zgonik, "Optical characterization of Al- and N-polar AlN waveguides for integrated optics," *Appl. Phys. Express* **8**, 042603 (2015).

²²L. Hussey, R. M. White, R. Kirste, S. Mita, I. Bryan, W. Guo, K. Osterman, B. Haidet, Z. Bryan, M. Bobea, R. Collazo, and Z. Sitar, "Sapphire decomposition and inversion domains in N-polar aluminum nitride," *Appl. Phys. Lett.* **104**, 032104 (2014).

²³R. Kirste, R. Collazo, G. Callsen, M. R. Wagner, T. Kure, J. Sebastian Reparaz, S. Mita, J. Xie, A. Rice, J. Tweedie, Z. Sitar, and A. Hoffmann, "Temperature dependent photoluminescence of lateral polarity junctions of metal organic chemical vapor deposition grown GaN," *J. Appl. Phys.* **110**, 093503 (2011).

²⁴P. K. Tien, "Light waves in thin films and integrated optics," *Appl. Opt.* **10**(11), 2395–2413 (1971).

²⁵D. Marcuse, "Mode conversion caused by surface imperfections of a dielectric slab waveguide," *Bell Syst. Tech. J.* **48**(10), 3187–3215 (1969).

²⁶R. Hunsperger, Theory and Technology in *Integrated Optics* (Springer New York, 1983), Vol. 15, p. 108.

²⁷I. H. Malitson, "Refraction and dispersion of synthetic sapphire," *J. Opt. Soc. Am.* **52**(12), 1377 (1962).